Detection of seasonal erosion processes cycles at the scale of an elementary black marl gully from time series of Hi-Resolution DEMs

J. Bechet[1]†, J. Duc[1], A. Loye[1], M. Jaboyedoff[1], N. Mathys[2], J.-P. Malet[3], S. Klotz[2], C. Le Bouteiller[2], B. Rudaz[1], J. Travelletti[3,*]

[1] {University of Lausanne, Risk-group - ISTE - Institute of Earth Sciences, Lausanne, Switzerland}

[2] {IRSTEA Grenoble, Unité de recherche Erosion Torrentielle, Neige et Avalanches, BP 76, 38402 Saint Martin d'Hères, France}

[3] {Institut de Physique du Globe de Strasbourg, CNRS UMR 7516, Ecole et Observatoire des Sciences de la Terre, Université de Strasbourg, 5 rue Descartes, F-67084 Strasbourg, France}

† Deceased on 28 March 2015

[*] {Now at: BEG - Bureau d'Etudes Géologiques SA, Rue de la Printse 4, CH-1994 Aproz}

Correspondence to: M. Jaboyedoff (Michel.Jaboyedoff@unil.ch)

1 Abstract

The Roubine catchment located in the experimental research station of Draix-Bléone (south French Alps) is situated in Callovo-Oxfordian black marls, a lithology particularly prone to erosion and weathering processes. Since 30 years, this small watershed (0.13 ha) has been monitored for analysing hillslope processes at the scale of elementary gullies.

Since 2007, a monitoring of surface changes has been performed by comparing of high-resolution digital elevation models (HRDEMs) produced from Terrestrial Laser Scanner (TLS). The objectives are 1) to detect and 2) to quantify the sediment production and the evolution of the gully morphology in terms of sediment availability/transport capacity vs. rainfall and runoff generation. Time series of TLS observations have been acquired periodically based on the seasonal runoff activity with a very high point cloud density

ensuring a resolution of the DEM at the centimetre scale. The topographic changes over a time span of 2 years are analysed.

Quantitative analyses of the seasonal erosion activity and of the sediment fluxes show and confirm that during winter loose regolith is created by mechanical weathering and it is eroded and accumulates in the rills and gullies. Because of limited rainfall intensity in spring part of the material is transported in the main gullies which are assumed as a transport-limited erosion system. In the late spring and summer the rainfall intensities increase allowing to wash out the regolith weathered and accumulated in the gullies and rills during the earlier seasons. Later in the year the catchment reacts as a sediment-limited system, because no more loose regolith is available. One interesting result is the fact that in the gullies the erosion-deposition processes are more active around the slope angle value of 35°, which indicates probably a behaviour close to dry granular material.

It is also observed that there exist thresholds for the rainfall events that are able to trigger significant erosion which are above 9 mm rainfall or intensity of more than 1 $mm.min^{-1}$, values which can vary if antecedent precipitations are significant within the last five days.

This study improves the knowledge of the spatial distribution of erosion seasonality in Badlands and demonstrates the potential of careful 3D hi-resolution topography using TLS to improve the understanding of erosive processes.

1 Introduction

This study is integrated in the cross-disciplinary research activities conducted in the Draix-Bléone catchments (SOERE-RBV: Systèmes d'Observation et d'Expérimentation pour la Recherche en Environnement-Réseau de Bassins Versants, i.e. network of catchments for the study of the critical zone, see portailrbv.sedoo.fr), composed of seven nested catchments characterized by several sizes and vegetation cover, this work focuses on the analysis of the processes controlling the annual pattern of erosion rates in elementary gullies (Richard, 1997; Meunier and Mathys, 1995; Mathys *et al*., 2005).

The region of Draix, where the study was conducted, is located within Jurassic black marls of Callovo-Oxfordian age (e.g. also called '*Terres Noires*') which cover large areas in South-East France. The Badlands landscape observed in these clay-shales catchments is the result of the conjunction of favourable lithological and climatic factors. Freeze–thaw and wetting–drying cycles progressively disintegrate the black marls formation thus favouring the annual development of a weathered marly layer exposed to surface runoff erosion and shallow landslides (Antoine *et al*., 1995; Maquaire *et al*., 2003). The weathered marls can be mobilized by Hortonian runoff especially during high-intensity rainfalls in summer. This causes flash floods and hyperconcentrated flows inducing significant problems in sedimentation reservoirs and river systems (Oostwoud Wijdenes and Ergenzinger, 1998; Descroix and Olivry, 2002). Saturation of the weathered marls layers can also locally trigger shallow landslides supplying high sediment loads to the basins. In addition, rain infiltration in the fractured marls bedrock contributes to the triggering of larger landslides whose geometry is controlled by the bedding and the discontinuities. There is a strong seasonal difference between the rates of surface erosion processes in summer and winter (Descroix and Gautier, 2002; Descroix and Mathys, 2003); the erosion processes have therefore an annually-cyclic activity pattern.

Terrestrial Laser Scanner (TLS) is a powerful tool to monitor erosion processes at the gully scale at a relatively low cost (Perroy *et al*. 2010; Jaboyedoff et al., 2012) where high spatial resolution data on surface changes is needed (Jacome, 2009). Such high resolution mapping of erosion rates at fine (e.g. seasonal) temporal scale for an entire catchment is innovative and represents considerable progress in the field of erosion assessment (Lopez Saez *et al*.,

2011). Preliminary studies show a great potential of TLS to measure and map surface erosion (Puech *et al*., 2009) since it can detect millimetre-scale changes at short-range distances (50 m; Abellán *et al*., 2009).

In this study, time series of intra-annual TLS observations are used to quantify surface erosion. The main objectives are: (i) to create erosion and deposition maps for every season; (ii) to estimate the sediment budget and evaluate the accuracy of the volume calculation at the catchment scale by comparing it to sediment trap observation and (iii) to propose a conceptual model describing the observed seasonal pattern of erosion and deposition. The results allow identifying and quantifying the topographic changes of the catchment in terms of regolith development, slope transfer processes, and transient storages of sediment within the rills and gullies. This is put in perspective with previous work on similar black marls slopes confirming the high impact of season on erosion processes cycles.

2 Physio-geographic settings of the study area: the Roubine catchment

2.1 Morphology

The research has been conducted in the Draix-Bléone experimental catchments (SOERE RBV network, *Systèmes d'Observation et d'Expérimentation pour la Recherche en Environnement Réseau de Bassins Versants*) in southeast France, near the city of Digne-les-Bains (Alpes-de-Haute-Provence). Draix-Bléone observatory is composed of seven small mountain watersheds. It was created by IRSTEA (Institut national de recherche en sciences et technologies pour l'environnement et l'agriculture) in 1983 in order to better understand erosion and sediment transfer processes, including hyperconcentrated floods, and to improve the design of protections in response to erosion processes. The experimental site selected for this work is the Roubine elementary catchment (Fig. 1), which is the smallest monitored (1330 m^2) watershed of the Draix experimental site (Mathys et al., 2003). No human actions have been conducted within the gully since the setup of the observatory in 1983.

This elementary watershed has a typical badland morphology characterized by V-shaped gullies, steep slopes (35 to 45°) and low vegetation coverage (ca. 20%). The Roubine elementary catchment is constituted by one main gully that crosses it from East to West.

This gully separates the catchment into a north- and a south-facing slope. On the south-facing slope, a secondary gully crosses diagonally in the direction North-east to South-west and confluences with the main gully at the catchment outlet. Both north and south-facing slopes are braided with many small gullies and rills of decametric widths. A few un-weathered marl outcrops can be observed in the steepest sections of both slopes. On these outcrops, the dip of the black marl formation is 25° to the East which has an impact on erosion processes (Esteves et al., 2005; Mathys et al., 2005). The scarce vegetation cover is constituted of a few black pines (*Pinus nigra*) and tuffs of grass restricted to the flatter interfluves near the sediment trap and on the top of the crests.

A sediment trap, a stream gauge and an automatic sampler are installed at the bottom of La Roubine in order to monitor the sediment yield and the water discharge (Mathys et al., 2003). Rainfall observations are collected by a rain gauge located 20 m from the Roubine outlet.

2.2 Geology

Large areas of Southeast France are covered by black marls which outcrop over more than 10.000 km^2 in the watershed of the Durance river (Légier, 1977; Phan and Antoine, 1994; Mathys *et al*. 1996). This sedimentary lithology is composed of alternating marl and limestone sequences whose ages range from Lias to Cretaceous. The marly sequence which outcrops in the Draix-Bléone catchments is from the Bathonian to Oxfordian, and its thickness can exceed 2000 m in some places (Antoine *et al*., 1995; Maquaire et al., 2003). These the black marls are overlain by limestones creating cliffs in the upper part of the Draix catchment (Ballais, 1999).

The mean erosion rate of the black marls averaged over 3 years (1985-1987) is 8 $mm.yr^{-1}$, which is approximately 100 $t.ha^{-1}.yr^{-1}$ (Olivry and Hoorelbeck, 1989), and more specifically of 100 $t.ha^{-1}.yr^{-1}$ or 13 $mm.yr^{-1}$ for La Roubine catchment.

2.3 Climate

The specific features of a Mediterranean mountain climate influence slope erosion rates with strong seasonal and yearly differences in temperature and rainfall. At Draix, the mean annual rainfall is 920 mm with an interannual variability of nearly 400 mm over the period

1970-2000. The summer is relatively dry, but several heavy thunderstorms can occur, which intensity sometimes exceeds 60 $mm.h^{-1}$ (Richard, 1997) and can even reach more than 100 $mm.h^{-1}$ during a few minutes (Yamakoshi et al., 2009), i.e. 210, 138, 90, 74 and 45 mm/h respectively during1, 5, 15, 30 and 60 minutes (Mathys, 2006). These events trigger hyper concentrated flows characterized by suspended sediment discharge of up to 800 $g.l^{-1}$ (Olivier, 1999). Micro-debris flows (MDFs) have also been observed (Oostwoud Wijdenes and Ergenzinger, 1998), and clearly associated with high erosive events (Yamakoshi et al., 2009; 2010). Hailstorms are not unusual. During spring and autumn seasons, the rainfall amounts are at their maxima. During the winter, very small amounts of rainfall are measured, but over 100 cycles of freezing-thawing are observed (Oostwoud Wijdenes and Ergenzinger 1998, Rovera and Robert, 2005). A snow cover can form but does not usually last the whole winter. The average yearly air temperature is 10.9 C with a standard deviation of 8.7°C (based on daily average temperature) over the period 1970-2000.

3 Methodology

3.1 Terrestrial Laser Scanner (TLS) measurements

The study site has been monitored using a Terrestrial Laser Scanning system (TLS). This remote scanning device is a monochromatic laser pulse transmitter/receiver. The laser beam pulses are oriented using mirrors or by moving the laser source mechanically or both. The time of flight (TOF) is the time for the pulses to travel the double distance (d), at the light velocity (c), to the reflecting surfaces ($2 \times d = c \times TOF$). In practice the laser has a footprint that increases in diameter with increasing distances to the target. The operation is repeated millions of times giving access to a very dense grid of XYZ points (Shan and Toth, 2008). Two types of TLS were used for this study: TLS1 is an Ilris 3D (Optech, Canada) scanner, and TLS2 is a TotalStation II (Leica, Germany) scanner. The TLS1 laser is infrared (1535 nm) and the performance coming from the manufacturer indicates that it produces data with an accuracy of 8 mm with a spot diameter of 22 mm at 100 m. The TLS2 laser is in the green wavelength (only information available from the manufacturer) with 6 mm accuracy and a 6 mm spot size at 50 m.

3.2 Data acquisition and processing

Twelve TLS campaigns were performed from 9th May 2007 to 4th November 2010 (Table 1). The data of the years 2007 and 2008 is sparser as the methodology and protocol were being developed. In 2009 and 2010, TLS data were acquired more regularly through the year in order to take into account more precisely the influences of the seasonal rainfall.

For each TLS campaign, the measures were performed from up to five different scan positions in order to minimize shadow areas. However, some shadow areas still remain because of the presence of foreground in the line of sight of the scanner or of vegetation. All scan spatial resolutions are less than 10 mm at a 50 m distance range. The point cloud density is very high for all the time series and ranges from 0.3 to 3 pts.cm^{-2}.

The software Polyworks V.10 (InnovMetric, 2010) has been used to process the TLS point clouds. First, the vegetated areas are deleted from the raw point clouds in order to keep for the analysis only the bare soil surface. The scans of each campaign are then aligned using the Iterative Closest Point (ICP) procedure (Chen and Medioni, 1992; Besl and McKay, 1992) to obtain a point cloud of the entire catchment. The TLS campaigns are aligned to a reference campaign (e.g. June 2009) using eight white 180 mm diameter styrene-spheres located around the catchment since 2008. Depending on the TLS distance of acquisition and the overlapping of the different scenes, the final point cloud density is variable; thus, each TLS point cloud has been interpolated using Surfer (GoldenSoftware 8) inverse distance method (Shepard, 1968) into a homogeneous high resolution (0.02 m) High Resolution Digital Elevation Model (HRDEM). A high-density point cloud produces an over-defined problem during the interpolation due to the too many points present in one grid cell (Schürch et al. 2011). If we do not consider the systematic error (that will be discussed separately later), the law of large numbers (Kromer et al., 2015) indicates that the accuracy will increase when average is performed, assuming that the surface is locally planar, at the centimetre scale. As an example, considering that the lower accuracy for one point is σ_1 = 8 mm. Performing an average on a surface area of 4 cm^2, (2 × 2 cm) with densities ranging from 0.3 to 3 pts.cm^{-2} (n = 1.2 and 12 pts in 4 cm^2) provides an accuracy ranging from 6.7 to 2.3 mm. Because σ_n is given by $(\sigma_1/n)^{0.5}$ assuming that the point cloud is well georeferenced. In some cases, TLS data can allow detecting movements below 1 mm, because of the law of large number (Kromer et al., 2015).

We do not consider horizontal error for two main reasons: (1) the effect of the slope orientation on the measures of point location very similar for each scan (the average slope does not change significantly between scans). (2) When merging scan with ICP the errors between scans include its horizontal components. It does not exceed the thresholds we used for detecting erosive processes (see sections 3.5 and 4.1). Assuming the systematic errors caused by slope orientation are similar (except for identified other problems) for all scans we are not tackling in more detail this topic.

3.3 Calculation of vertical difference HRDEMs: location of erosion-prone areas and quantification of volume changes

To quantify and map the erosion and deposition through time, the most recent HRDEM was subtracted from an earlier HRDEM (DeRose et al., 1998). The resulting elevation changes have negative pixel values representing erosion and positive pixel values representing deposition.

Eleven differences between successive HRDEMs providing DEMs of Differences (DoDs) have been calculated from the 9th May 2007 to the 4th November 2010 (Fig. 2). Because the occurrence of processes is strongly related to each season, the HRDEMs are sorted out by seasonal periods. The mapping of the different erosion and deposition areas is carried out for each season by taking into account the DoDs of the corresponding seasons. These comparisons allow the detection and mapping of the most erosion-deposition-prone areas in the catchment (Fig. 3), and the characterization of the annual pattern of erosion (Betts and DeRose, 1999). These maps represent a synthesis of the DoDs (Fig. 2) showing the erosion or deposition areas. On these maps (Fig. 3), the erosion areas are displayed in orange and the deposition areas are in blue (see also the video in the supplementary material).

To quantify the volume of soil surface changes, the elevation differences are summed and multiplied by the DEM squared cell resolution (0.004 m^2). To obtain the sediment budget, the total volume of deposition is subtracted from the total volume of erosion. This calculation provides the final results of topographic changes in cubic meters. To minimize scan alignment inaccuracy on the quantification of the volumes, the topographic changes outside the active erosion–prone areas previously mapped have been ignored. Finally, an

228 average density of 1500 kg.m^{-3} for the black marls deposits measured in the sediment trap
229 as proposed by Mathys *et al*. (1996). In addition, the volumes of sediment deposited in the
230 sediment trap have been increased by 20%. Because the annual an average of 20% of the
231 total eroded sediment exits the catchment in water-suspended flows (Mathys, 2006). It must
232 be noted that during major storm events, up to 40% of sediments can exit the catchment in
233 hyperconcentrated flows (Mathys, 2006). The corrected volumes are obtained using these
234 two values and the results are used to calibrate the TLS volumes in order to take into
235 account the expansion. This has been performed because some vegetated areas and some
236 occlusions exist which are not imaged by the scans (Table 2 and 3). As reminder this
237 occurred because the access within the Roubine catchment is forbidden. This allows also
238 to get a rough idea of the density of the eroded material. It changes throughout the year
239 according to the seasons indicating that in summer the density is close to the bedrock value
240 (i.e. 2325 kg.m^{-3}) and during spring it close to the sediment 1500 kg.m^{-3}.

241 ### 3.4 Slope gradient and aspect

242 In order to evaluate the role of topographic proxies (slope angle, slope aspect, upstream
243 contributing area (UCA), TOBIA index (Meetenmeyer & Moody, 2000)), the DoDs of each
244 period are averaged on a 10 cm grid to reduce noisy values. Several topographic parameters
245 are computed on the June 2010 topography, using ArcGIS (slope angle, aspect and
246 upstream contributing area) and Matlab (TOBIA). Gullies are identified as pixels with
247 UCA values over 10 m^2 with a 20 cm buffer to account gully width. This discriminate
248 slopes from gullies.

249 The TOBIA index is computed assuming a uniform dip and dip direction of the black marls
250 at 25°/86°, as observed on the field and computed using Coltop software (Jaboyedoff et al.
251 2007).

252 ### 3.5 Sources of errors

253 The use of TLS observations resulted in several sources of errors that were quantified. First,
254 TLS measurements are affected by instrumental errors as described by Abellán et al.
255 (2009). These authors showed in particular that when averaging point clouds the detection
256 of changes improved significantly. Second, some scans are also affected by deformation
257 due to atmospheric conditions. Third, some DoDs contain some misalignment

characterized by slight tiling due to scan deformation and/or scan alignment inaccuracies; such a source of error is for instance clearly visible on Fig. 2F. The use of a high threshold value to validate DoDs values to detect process of erosion or deposition permits to escape from the problems of misalignment or atmospheric deformation (see below). In fact, the quality precision and precision of the two successive alignment procedures, i.e. the scan merging and the "georeferencing" vary from a measurement campaign to another as the TLS instrument, the scan deformation and the spatial resolution were different (Table 2).

A possible procedure to estimate the overall errors is to define the quality of the alignments for each campaign (1) and between them (2). This corresponds to the measures of the dispersion of the points between two merged scans (1). This is performed by identifying the areas that have not changed (fixed surfaces like the spheres, wall, etc.). The average distance between two scans and the associated standard deviation is performed using the point to surface method. (2) Similar procedure can be applied to successive campaigns. Note that the averaging of the HRDEM allows reducing the noise and minimizing other measurement errors.

4 Results

4.1 Analysis of soil surface height differences

DoDs outline the slope surface changes at a centimetre scale (Fig. 2). All the DoDs are presented in a plan view on a hillshade of the watershed. The eastern limit of the catchment lacks in data because of a dense vegetation cover. The differences under 1.8 cm are not displayed. This limit has been chosen on a trial and error procedure, and assuming that it contains in most cases above three times the maximum error of alignment of 6 mm, except for the scans of 2007. A clustering of the height differences in three classes is proposed both for the erosion and deposition; small height differences ranging from 1.8 to 4.0 cm, moderate height differences ranging from 4.0 to 10.0 cm, high height differences above 10.0 cm in absolute value. The erosion pattern is displayed in warm colours while the deposition pattern is displayed in cold colours.

4.2 Cartography and temporal pattern of erosion processes

Five erosion patterns are distinguished for La Roubine catchment; winter, spring, late spring - early summer, summer and autumn:

- Winter seasons erosion pattern is illustrated by the DoDs between the 3rd November 2009 and the 23rd March 2010 (Fig. 2G).
- Spring seasons erosion pattern is represented by DoDs between the 14th April to the 1st June 2009 and the 23rd March to the 28th May 2010 (respectively Figs. 2D and 2H);
- The erosion pattern of late spring - early summer rainy season is illustrated by the DoDs between the 9th May 2007 to the 24th June 2007 and the 28th May to the 23rd June 2010 (respectively Figs. 2A and 2I). In 2009, the rainfall amount at this season was 30% below average up to 20th December, and 19% below average for the whole year, only thanks to some late precipitations in the last days of the calendar year, most probably snow. Thus no DoD corresponds for that period in 2009;
- Summer season erosion pattern is represented by DoDs between the 1st June to the 11th August 2009 and the 23rd June to the 22nd September 2010 (respectively Figs. 2E and2 J);
- Autumn season erosion pattern is represented by DoDs between the 11th August to the 3rd November 2009 and the 22nd September to the 4th November 2010 (respectively Figs. 2F and 2K).

During winter seasons, (Fig. 3E) the alternating freezing-thawing cycles favour the regolith development. Gelifluction (and solifluction during thawing) in the upper parts of the gullies and on the steep slopes surrounding the gullies lead to an accumulation of material in the lower parts of the gullies. The soil surface changes are mostly located on the south-facing slopes of the watershed. Higher number of freezing-thawing cycles result in a higher amount of regolith that can be mobilized (Maquaire et al., 2002; Raclot et al., 2005) and therefore more production of sediment along the slopes.

During the spring seasons, (Fig. 3A), the sediment accumulated during winter in the main gullies is transported at the outlet of the catchment. This transport is generally limited to the two main gullies. Erosion is transport-limited and consequently only the gullies with the larger contributing surface are drained.

During late spring – early summer rainy seasons, (Fig. 3B), the rainfall can be relatively intense (Mathys et al., 2005). Consequently, the secondary rills, gullies and the steepest slopes can be strongly affected by Hortonian runoff and the weathered regolith developed during winter can be washed out. The south-facing slopes are more prone to such type of erosion pattern as more weathered sediment is produced during winters. Often, small deposition levees are observed at the lower (flatter) parts of the gullies.

During the summer seasons (Fig. 3C), characterized by relative drought except the occurrence of a few thunderstorms, there is very little erosion activity. The same small gullies and rills than those affected by the late spring erosion pattern are continued to be eroded in their steepest parts while deposits and small levees are formed in their lower parts. Most of the loose weathered regolith has already been washed away. The less frequent but more intense storms observed in this season do not impact the erosion pattern, now sediment-limited.

During the autumn seasons (Fig. 3D), the rainfall pattern is characterized by long and low intensity events with some very short intense precipitations prone to a slow soil wetting and consecutive increase in soil moisture. Progressively, a new layer of regolith is created, and in most of the rills and gullies, sediment transport is reactivated.

4.3 Topographic influences

DoDs values changes overs time are plotted against topographic proxies. The DoDs values are displayed for slopes (top) and gullies (bottom) for each period (Figs. 4-6; in supplementary material similar figures provide DoDs values plotted against topographic proxies).

The seasonal cycle is clearly visible on the slope angle vs DoDs rate of changes (Fig. 4), with the deposition/erosion cycle during the year and regolith expansion. Autumn and winter periods see accumulation of loose sediments in the gullies, which are then eroded in late spring or early summer. We can suspect that in winter it is a slow continuous process and in late spring early summer it suffer pulse of erosion (it can be also an artefact because of the unequal time between surveys). In those gullies, both maximum deposition (November to March) and erosion (March to May) are reached at a slope angle of 35°, a critical slope for granular material (Gotzinger et al., 2007) and thus also the deposits most

susceptible to erosion. The summer and autumn periods show limited change, both in gullies and slopes.

The slope aspect proxy (Fig. 5) also shows the annual cycle and separate behaviour between slopes and gullies. South and southwest facing slopes are more susceptible to increased erosion/deposition, probably expansion (particularly November to March and June to September periods).

Upstream contributing area show the same seasonal pattern, with deposition (gullies) and expansion (slopes) in winter and erosion in early summer. From June to September, DoD values are inversely proportional to UCA in slopes, with gullies showing smaller changes (Fig. 6).

TOBIA index values show that the Roubine gully is mainly composed of orthoclinal slopes (52% of area) and steepened escarpments (39% of area), consistent with its east-west incision into east-dipping marls, but no link can be seen between erosion activity and structural outcropping conditions. Intersection between bedding and topography is very similar across the whole catchment.

4.4 Quantification of seasonal sediment budget changes

For the quantification of the seasonal sediment budget changes, the TLS data of the years 2007 and 2008 have been ignored, because TLS data were not covering the largest possible area of the catchment as other did. The eroded volumes trend estimated with TLS (Table 2) are in agreement with the integrated measurement of coarse sediment transfer at the outlet trap (Table 3; Fig. 7). The difference is in an acceptable range (5.5% for the period from 14.04.2009 to 4.11.2010 on the total cumulated volumes).

The maximum eroded volume is produced for the period March-June 2010 (Table 2) with a sediment transfer of ca. 8.7 m^3 (35 m^3/year or 26 mm/year) out of the catchment. For the period November 2009-March 2010 (Table 2) more than 1.2 m^3 (3.1 m^3/year or 2.3 mm/year) are transported but most of the volume is redistributed within the catchment because the rainfalls were not intense enough to transport the sediments out of the catchment. The autumns 2009 and 2010 (Table 2) are characterized by moderate sediment transfers with respectively 0.9 m^3 (4.1 m^3/year or 3.1 mm/year) and 1.6 m^3 (13.7m^3/year or

10.3 mm/year) transported out of the catchment based on TLS observations, with some significant rainfall events. It must be noted that the event of the 21 October 2009 led to a deposit of 1.7 m^3 (more than 1 cm eroded over the whole catchment) in the sediment trap, with an intensity reaching 0.8 $mm.min^{-1}$ and rain totalling 36 mm during the day. The three main events of 2010 are of different types. The first occurred during the 14 first days of May for a total of precipitation of 155 mm. The main precipitation event occurred on 10^{th} of May, which reached 1 $mm.min^{-1}$ (during four minutes more than 0.5 $mm.min^{-1}$) after antecedent precipitations since May 1 of 70 mm. A volume of nearly 3 m^3 was transferred out of the catchment during that period. The second occurred on the 15^{th} June 2010 with a daily rainfall of 69 mm, with the day before 5.5 mm including an intensity maximum of 0.8 $mm.min^{-1}$. The maximum intensity of the 15^{th} was of 0.6 $mm.min^{-1}$ after 42 mm of antecedent precipitation (from the 14 of June). It appears that this event was able to transport out of the catchment around 3 m^3 measured in the trap and estimated at 6 m^3 from TLS for the period 28.05-23.06.2010. The last important event occurred on 4 October 2010, with a small but intense 12 mm rain event. The intensity reached 1 $mm.min^{-1}$ during 10 minutes. The measurements by TLS (1.6 m^3) and within the sediment trap (1.7 m^3) were very close.

5 Discussion

5.1 Interpretation

With the TLS measurements, the balance value is negative when the erosion sediment volume is larger than the deposited sediment volumes. The presence of shadow areas in the TLS scans affects the TLS sediment budget as erosion-prone areas can be hidden from the laser pulse. When these erosion-prone areas are hidden, the deposited sediments can be estimated as more important than the erosion volumes. The balance is therefore positive, as for example for the period June-September 2010 (Table 2). The shadow areas are usually located in the upper parts of the slopes, often very steep and close to the crests of the catchment; these areas are highly productive sources of sediments Therefore, it is hypothesized that the sediment budget is underestimated for most of the periods. The value of eroded volumes based on sediment trap is increased by 20% to include the suspended sediments otherwise the true erosion rates are underestimated. In addition, although the

swelling or inflation of the regolith surface (Bechet et al., 2015) can have an influence on the georeferencing, it was not possible to quantify it at the level of La Roubine catchment. Nevertheless, it has been shown that the un-weathered black marls density is 2650 $kg.m^{-3}$, while the regolith density can be as small as 1300 $kg.m^{-3}$ but it varies greatly in space and time according to the presence of local discontinuities (Maquaire et al., 2003; Travelletti et al., 2012). The measurements of the densities of the black marl deposited in the sediment trap vary usually from 1500 $kg.m^{-3}$ to 1800 $kg.m^{-3}$ (Mathys *et al*., 1996). By calibrating the TLS with sediment trap volume, the swelling or inflation of the regolith has been indirectly quantified by the observed changes of eroded material density. The density of the regolith when it is in mostly disturb state possesses a density of 1500 kg/m^3, which makes ~75% of volume increase compared to the bedrock density 2650 kg/m^3. And 2325 kg/m^3 corresponds to an expansion of 14%. For the lowest measured value 1300 kg/m^3, the increase is more than 100%. In addition, the slope-erosion relationship shows some positive values in winter, indicating an increase of volume.

Also, topographic height differences smaller than the TLS threshold of 1.8 cm, are not integrated in the sediment budget while they could contribute to an important sediment volume because of their possible widespread occurrence, mainly during the summer storms that trigger important Hortonian runoff. This limitation also influences the sediment budget by underestimating the total volume of erosion. But because of the coherence of the results, we consider that it can be a base for an interpretation of the catchment erosional system.

5.2 Conceptual model

All the results can be synthesized in a conceptual model describing the seasonal pattern of erosion and deposition and quantifying the volumes of sediment transfer (Fig. 8). This seasonal pattern is controlled by the rainfall distribution and the availability of sediment during each period. The results may thus be different depending on the year but the sequence will not change, only the time lapses between major erosive events will change.

During the spring and summer seasons, the sediment transfer consists of the erosion of the weathered loose regolith layer on the slopes and a mobilization of the transient storages of accumulated sediments in the rills and gullies (bottom row of Figs. 4, 5 and 6), if no exceptional rainfall event occurs. But during the late spring and early summer intense

436 rainfall event produce very high erosive events (Figs. 4, 5 and 6 and in supplementary
437 material). Most of the sediments exiting the Roubine catchment are a product of the winter
438 weathering. It appears has a slow process, rates of change smaller than in the other periods,
439 but longer and as a consequence the total changes are important, but is can be an artefact
440 due to the time period between surveys (see and compare Figs. 4-6 and in supplementary
441 material). The erosion progressively evolves from a transport-limited (at the beginning of
442 spring) to a supply-limited one (in summer) pattern. However, diffuse erosion may happen
443 during intense summer storms as heavy drops may detach and displace small particles,
444 creating sparse local erosion and deposition. Hortonian runoff may also be generated, but
445 its effects could not be measured with the TLS technique as a higher accuracy is necessary.
446 In the autumn seasons, a new layer of loose regolith is progressively created (Fig. 4, top
447 row), and if an intense rainfall event has occurred before in summer as it is usually the case,
448 then the quantity of available sediment is limited (Figs. 4, 5, 6, bottom rows).

449 The main events summarized above all occurred after more than 9 mm rainfall, which is
450 also the limit for initiating runoff in a larger similar catchment (Laval) after more than 5
451 antecedent dry days (Mathys et al., 2000). That threshold is lower if the dry period is
452 smaller than 5 days. These events possess either intensity that reaches 1 $mm.min^{-1}$ (=60
453 $mm.h^{-1}$), which is the limit to trigger MDF's (Yamakoshi et al., 2009) or with immediate
454 antecedent rainfall that has saturated the soil. This last situation permits to initiate earlier
455 the runoff, if it is coupled with significant precipitation, which permits to induce an erosion
456 pulse with lower intensities such as 0.6 $mm.min^{-1}$. The sediment yield is controlled by the
457 availability of the upper part of regolith and by the grain size distribution. Mathys (2006)
458 indicated that in the area of Draix the four first centimetres of the regolith contain 45% clay
459 and silts and 4-8 cm contains 35% clays and silts. This shows that the size of material
460 transported will change with time, i.e. antecedent period in terms of rainfall and climate.
461 In addition, it has been shown that in the beginning of the year the sediment moves but stay
462 partially within the catchment, concentrating the material in the gullies. This non-linearity
463 is supported by the fact that the quantity and type of material mobilized depends on the
464 duration and intensity of the rainfall. Partitioning of the total load exported from the
465 catchment shows that at low discharge the suspended material part ranges between 0 and
466 40%, whereas it is close to 40% for higher discharge (Mathys, 2006). This indicates that

only high intensity precipitations can mobilize the whole upper part of the regolith and/or split marl plates in smaller particles, whereas small intensities depend on the grain size of this upper part of the regolith at the time of the event.

It is also clear that sediment transfer depends on the material available (Bardou and Jaboyedoff, 2008). The winter period, because of frost/thaw cycles and low rainfall intensity, permits to create and accumulate weathered material. The relatively low rainfall intensities of these winter periods permit to mobilize partially material that remains within the slope and gullies. It is also interesting to note that the most active zones, both in erosion and deposition, within the gullies are located around a slope angle of 35°, which corresponds to the angle of repose or dry granular material (Gotzinger et al., 2007). This indicates that sediment transfer from the slopes to the gullies is mostly controlled by local dry transport.

The difference between rills and inter-rill erosion depends on rainfall intensity, and antecedent rainfall amounts. The accumulated material in the rills can be mobilized by moderate rainfall intensities for fine material, while inter-rills need intense precipitations and/or a well-developed upper part of the regolith. In winter, the upper regolith probably only moves on short distance at centimetre scale by small mass movements (Bechet et al., 2015) and at meter scale by MDFs. In spring, the material accumulated in the rill is washed away, and later the inter-rills and rills with small contributing areas can be eroded and the material transported outside the catchment. Autumn permits to clean the material accumulated during summer in the main rills. This scheme may change depending on the future climate, if less precipitation occurs and only intense rainfall event remains. The system could then concentrate the full erosion in one or a few events. A warmer climate may also reduce the number of frost-thaw cycles and thus also reduce the depth of the regolith layer generated every year. But in any case the seasonality that leads to weathered material will remain in the cold period, which is the main producer of sediments that can be mobilized.

5.3 Hillslope activity processes

The observed high production of loose regolith is mainly caused by the alternating of freezing-thawing and wetting-drying cycles, which is the key process controlling the

497 weathering of black marl slopes (Maquaire et al., 2002; Brochot et Meunier, 1994). At the
498 end of the winter season, a thick layer of loose regolith can be accumulated in the areas of
499 the slopes and gullies with slope angles around 35°. The south-facing slope is characterized
500 by a higher number of weathering cycles than the north-facing slope (Maquaire et al., 2002)
501 leading to the observed more active erosion/deposition processes. Because considering
502 only the freezing and thaw cycles the south-facing slopes suffer more cycles than the north-
503 facing ones, but the gullies located in the south-facing slope are equivalent to north facing
504 slope (Rovera and Robert, 2005). However, the north-facing slopes present higher depths
505 of frozen soils. In addition, it has been demonstrated that erosion rates increase with
506 increasing slope angle on bare marls (Lopez-Saez et al., 2001). This is not clearly the case
507 here, in fact the regions close to gullies are more subject to erosion because of previous
508 accumulation. In addition, the structures can play a role. The slopes cutting the bedding by
509 an angle close to 90° are more prone to erosion than in dip slope or following the top of
510 bedding (Esteves et al., 2005). This is mainly caused by the alternation of more competent
511 and weaker bedding, which controls the first one. Dip slopes are less sensitive to weak
512 layers except if they are outcropping at the top. However, this behaviour cannot be
513 confirmed in La Roubine, as not all outcropping types are present.

514 Another point is runoff seasonal changes. It is transport-limited in spring, which is probably
515 mainly caused by the limited amount of intense rainfall during this season. Looking at the
516 flow accumulation values, the gullies that have a contributive area smaller than 100 m^2 are
517 not able to mobilize material if the daily rainfall or the intensity is not sufficient. To give
518 an order of magnitude, if an intense event of a few minutes at 0.5 $mm.min^{-1}$ occurs on a
519 saturated ground (on these 100 m^2), and assuming 100% runoff, the discharge will be of
520 0.5 $l.min^{-1}$ which probably permits to erode the rills. In addition, the effect of runoff and
521 rainfall intensity is not straightforward. The erosion rate depends first on the material
522 available, second on the rainfall intensity and third on the slope. Summer season does not
523 include the two first conditions. But low intensity rainfalls are participating to the cycle of
524 erosion by allowing drying and wetting plus micro-slope movements, which weather the
525 regolith more and transfer mass locally. As we observed the slope surfaces evolve
526 dynamically through the yearly cycle. In the spring season, the regolith observed in the
527 gullies has a popcorn structure defined as “Expansion [...] accompanied by the

development of cracks separated by micro-humps" (Gutiérrez, 2005), and therefore a lower density compared to the unweathered black marls. In the summer season, sedimentary and structural thin crusts can develop at the surface of the regolith because of the intense wetting (Malet et al., 2003). In the absence of shallow mass movements, the lower part of the slopes are, generally, eroded by runoff at the same rate as the interfluves and the upper part the slopes; this system yields to relatively constant slope gradient values over time (Descroix and Mathys, 2003).

6 Conclusion

By their strong and rapid responses to climate forcing, the black marls of Draix-Bléone are favourable to the analysis of erosive processes. This article confirmed results of previous works. The strong dependence to the seasons and the cycle of processes (Jacome 2009) or the sediment trap measurements and the density of the regolith (Mathys 2006). The prediction of the responses of small mountain watersheds to climatic events is improved.

TLS has proved to be an appropriate tool to monitor gully erosion while being easily reproducible and accurate all at once. It also allowed working at the centimetre scale with success. The method used to create and compare DEMs proved very effective to map and quantify topographic changes, but some difficulties have still to be solved to fully quantify the sediment transfer.

The TLS permits mainly to locate the different processes. This first results are showing that the rainfall pattern, i.e. time-series, intensity and duration, controls the sediment delivery sequence, but the process of weathering (mainly freezing and thawing) is fundamental to provide material for either suspended load or bed load. The interplay of rainfall and weathering creates the seasonal pattern. The complete erosion processes seems to imply during winter and slow transport-limited processes by weathering (swelling), but they affect important volumes, later in summer the behaviour is sediment-limited. While from late spring to early summer the erosion is very intense controlled by pulses induced by intense rainfalls. Further investigation could also focus on the dry granular transport and its role for the accumulation of sediments during winter periods.

Here we have shown the limits of the methods. Further investigations with HRDEM must be carefully set up in order to avoid the error coming from data acquisition. In addition, these surface monitoring must be coupled with more variables monitored during the event simultaneously such as soil moisture, the swelling, rain drop size, the grainsize distribution, the soil density, etc. Furthermore, density map of the regolith inside the catchment throughout the year (season by season) would be a great help to improve the TLS volume correction, but this will require to intervene physically in the catchment to install sensors and collect samples.

Such procedures are not possible in the Roubine catchment, which must not be perturbed by human activity. A new small catchment (Roubinette) has thus been instrumented on the site of Draix, which will permit to install instruments inside the watershed itself. Another next step will be to acquire TLS data during a storm event.

7 Acknowledgments

To the IRSTEA who let us work on his field and who gave us precious data. Thanks to the GIS Draix and particularly to S. Klotz (IRSTEA). We dedicate this paper to the first author Jacques Bechet, who died in a snow avalanche 28 March 2015. The content of this paper is an expression of his great ingenuity, curiosity and research spirit he shared with his co-worker Julien Duc. We will ever remember his enthusiasm.

References

Abellan A., Jaboyedoff M., Oppikofer T., Vilaplana J.M.: Detection of millimetric deformation using a terrestrial laser scanner: experiment and application to a rockfall event, Natural Hazards and Earth System Science. Hazards Earth Syst. Sci., 9, 365–372, 2009.

Antoine P., Giraud A., Meunier M., van Asch Th.W.J.: Geological and geotechnical properties of the ‘Terres Noires’ in southeastern France: weathering, erosion, solid transport and instability, Engineering Geology, 40, 223-234, 1995.

Ballais J.-L. : Apparition et évolution du modelé de roubines dans les Préalpes du Sud : l'exemple de Draix, CAGÉP - URA 903 du CNRS, Institut de Géographie de l'Université de Provence, 1999.

585 Bardou E. and Jaboyedoff M.: Debris Flows as a Factor of Hillslope Evolution controlled
586 by a Continuous or a Pulse Process? In: K Gallagher, S. J. Jones and J. Wainwright:
587 Landscape Evolution: Denudation, Climate and Tectonics over Different Time and
588 Space Scales. Geol. Soc. London Spec. Publ., 63-78, 2008.

589 Bechet J., Duc J., Jaboyedoff M., Loye A. and Mathys N.: Erosion processes in black marl
590 soils at the millimetre scale: preliminary insights from an analogous model. Hydrol.
591 Earth Syst. Sci., 19, 1849–1855, doi:10.5194/hess-19-1-2015, 2015.

592 Besl P. J. and McKay N. D: A method for registration of 3-d shapes, IEEE Trans. Pat. Anal.
593 and Mach. Intel., 14(2), 239–256, 1992.

594 Betts H.D. and DeRose R.C.: Digital elevation models as a tool for monitoring and
595 measuring gully erosion. JAG, 1, 3, 91-100, 1999.

596 Brochot S. and Meunier M.: Erosion de badlands dans les Alpes du Sud –Synthèse-,
597 CEMAGREF division protection contre les érosions, mars 1994. 1994.

598 Chen Y. and Medioni, G. : Object modeling by registration of multiple range images.
599 Image Vis. Comput. 10, 145-155, 1992.

600 DeRose R.C., Gomez B., Marden M., Trustrum N.A.: Gully erosion in Mangatu Forest,
601 New Zealand, estimated from digital elevation Models, Earth Surface Processes and
602 Landforms, 23, 1045-1053, 1998.

603 Descroix L. and Olivry, J.C. : Spatial and temporal factors of erosion by water of black
604 marl in the badlands of the French Southern Alps. Hydrological Sciences Journal 47 (2),
605 227–242, 2002.

606 Descroix L. and Gautier E.: Water erosion in the southern French Alps: climatic and human
607 mechanisms, Catena 50, 53-85, 2002.

608 Descroix L. and Mathys N.: Processes, spatio-temporal factors and measurements of
609 current erosion in the French southern Alps: A review, Earth Surface Processes and
610 Landforms 28(9): 993-1011, 2003.

611 Esteves M., Descroix L., Mathys N., Lapetite J. M.: Soil hydraulic properties in a marly
612 gully catchment (Draix, France). Catena, 63, 282-298, 2005.

613 Grotzinger J. and Jordan T.H, Press F., Siever R.: Understanding Earth, 7th ed. Macmillan,
614 579 p., 2007.

615 Gutiérrez, M., Climatic Geomorphology. Elsevier, Amsterdam, 760 p., 2005.

616 Innovmetric Software Inc.: Polyworks, version 9.1.8. http://www.innovmetric.com, 2010.

617 Jaboyedoff M., Metzger R., Oppikofer T., Couture R., Derron M.-H., Locat J., Turmel D.:
618 New insight techniques to analyze rock-slope relief using DEM and 3D-imaging cloud
619 points: COLTOP-3D software. In Eberhardt, E., Stead, D and Morrison T. (Eds.): Rock
620 mechanics: Meeting Society's Challenges and demands (Vol. 1), Taylor & Francis. pp.
621 61-68, 2007.

622 Jaboyedoff M., Oppikofer T., Abellán A., Derron M.-H., Loye A., Metzger R., Pedrazzini
623 A.: Use of LIDAR in landslide investigations: a review. Natural Hazards, 61:5–28, DOI
624 10.1007/s11069-010-9634-2, 2012.

625 Jacome A. : MNT à très haute résolution spatiale pour la représentation 3D des ravines
626 d'érosion de montagne, Thèse de Doctorat, Université Montpellier II, Sciences et
627 Techniques du Languedoc, 2009.

628 Kromer R, Abellán A., Hutchinson J., Lato M., Edwards T. and Jaboyedoff M. : A 4D
629 filtering and calibration technique for small-scale point cloud change detection with a
630 Terrestrial Laser Scanner. Remote Sens. :7(10), 13029-13052; doi:10.3390/rs71013029,
631 2015.

632 Légier, A. : Mouvement de terrain et évolution récente du relief dans la région de
633 Barcelonnette (Alpes-de-Haute-Provence). PhD thesis, Grenoble I University. 163 pp.,
634 1977.

635 Lopez Saez J., Corona C., Stoffel M., Rovéra G., Astrade L., Berger F.: Mapping of erosion
636 rates in marly badlands based on a coupling of anatomical changes in exposed roots with
637 slope maps derived from LiDAR data, Earth sruface Surface processes Processes and
638 landformsLandforms, DOI: 10.1002/esp.2141, 2011.

639 Malet J.-P., Auzet A.V., Maquaire O., Ambroise B., Descroix L., Esteves M., Vandervaere
640 J.-P., Truchet E.: Investigating the influence of soil surface features on infiltration on
641 marly hillslopes. Application to callovo-oxfordian black marls slopes in the

642 Barcelonnette basin (Alpes-de-Haute-Provence, France). Earth Surf Proc Land
643 28(5):547–564, 2003.

644 Maquaire O., Malet J.-P., Remaître A., Locat J., Klotz S., Guillon J.: Instability conditions
645 of marly hillslopes: towards landsliding or gullying? The case of the Barcelonnette
646 Basin, South East France. Engineering Geology 70, 109–130, 2003.

647 Maquaire O, Ritzenthaler A., Fabre D., Thiery Y., Truchet E., Malet J-P., Monnet J. :
648 Caractérisation des profils de formations superficielles par pénétrométrie dynamique à
649 énergie variable : application aux marnes noires de Draix (Alpes-de-Haute-Provence,
650 France). Comptes-Rendus Geosciences, 334, 835-841, 2002.

651 Mathys N., Brochot S. and Lacheny B. :Genèse des crues et érosion dans les petits bassins
652 versant de montagne : observations et résultats obtenus sur les bassins versants
653 expérimentaux de Draix (Alpes-de-Haute-Provence). Association Forêt
654 Méditerranéenne : XXI (2), 182-190, 2000.

655 Mathys N. : Analyse et modélisation à différentes échelles de mécanismes d'érosion et de
656 transport de matériaux solides. Cas des petits bassins versants de montagne sur marne
657 (Draix, Alpes-de-Hautes_Provence), PhD Thesis, Institut National Polytechnique de
658 Grenoble, 2006.

659 Mathys N., Brochot S., Meunier M.: L'érosion des terres noires dans les Alpes du Sud :
660 contribution à l'estimation des valeurs annuelles moyennes (bassins versants
661 expérimentaux de Draix, Alpes-de-Haute-Provence, France), CEMAGREF, Grenoble,
662 1996.

663 Mathys N., Brochot S., Meunier M., Richard D. : Erosion quantification in the small marly
664 experimental catchment of Draix (Alpes Alpes-de de-Haute Haute-Provence, France).
665 Calibration of the ETC rainfall-runoff-erosion model, Catena 50, 527-548, 2003.

666 Mathys N., Klotz S., Esteves M., Descroix L., Lapetite J.-M.: Runoff and erosion in the
667 Black Marls of the French Alps: observations and measurements at the plot scale,
668 Catena 63, 261-281, 2005.

669 Meentemeyer R.K., Moody A.: Automated mapping of conformity between topographic
670 and geological surfaces, Computers and Geoscience 26, 815-829, 2000

671 Meunier M., Mathys N.: Panorama synthétiques des mesures d'érosion effectuées sur trois
672 bassins du site expérimental de Draix (Alpes-de de-Haute Haute-Provence, France),
673 CEMAGREF, Grenoble, 1995.

674 Olivier J.E. : Les fortes crues d'août 1997 à Draix : d'un printemps sec à des records de
675 charges solides, Les bassins versants expérimentaux de Draix laboratoire d'étude de
676 l'érosion en montagne - actes du séminaire, Draix Le Brusquet Digne, 22-24 octobre
677 1997. Cemagref Editions, Antony, pp. 53-63, 1999.

678 Olivry J.-C., Hoorelbeck J. : Erodibilité des terres noires de la vallée du Buëch (France,
679 Alpes du Sud). Cahiers ORSTOM.Série Pédologie: 25 (1-2), 95-110. ISSN 0029-7259,
680 1989.

681 Oostwoud Wijdenes D.J., Erzinger P.: Erosion and sediment transport on steep marly
682 hillslopes, Draix, Haute-Provence, France: an early experimental field study, Catena 33,
683 179-200, 1998.

684 Perroy R. L., Bookhagen B., Asner G. P., Chadwick O. A.: Comparison of gully erosion
685 estimates using airborne and ground-based LiDAR on Santa Cruz Island, California,
686 Geomorphology 118, 288–300, 2010.

687 Phan, T.S.H. and Antoine, A.: Mineralogical and geotechnical characterization of the
688 ''Black Lands'' of the South-East of France, having in view road applications.
689 Proceedings of the VIIth International Congress of the Intenational Association of
690 Engineering Geology, Lisboa, vol. 2. Balkema, Rotterdam, pp. 961– 966, 1994.

691 Poesen J., Nachtergaele J., Verstraeten G., Valentin C.: Gully erosion and environmental
692 change: importance and research needs, Catena 50, 91-133, 2003.

693 Puech C., Thommeret N., Kaiser B., Bailly J.-S., Jacome A., Rey F., Mathys N.: MNT à
694 très haute résolution dans les modelés fortement disséqués : des données aux tests
695 d'application, Géomorphologie 2/2009, 2009.

696 Raclot D., Puech C., Mathys N., Roux B., Jacome A., Asseline J., Bailly J.-S. :
697 Photographies aériennes prises par drone et modèle numérique de terrain : apports pour
698 l'observatoire sur l'érosion, Géomorphologie (2005), 7-20, 2005.

Richard D. : les Les bassins versants experimentaux expérimentaux de Draix (04) : éetude de l'érosion et du transport solide torrentielle à partir de mesures in situ, CEMAGREF, Grenoble, 218-228, 1997.

Rovera G. and Robert, Y.: Conditions climatiques hivernales et processus d'érosion périglaciaires dans les badlands marneux de Draix. GEographie Physique et Quaternaire, 59 (1), 31-48, 2005.

Schürch P, Densmore A.L., Rosser N.J., Lim M., McArdell B.W.: Detection of surface change in complex topography using terrestrial laser scanning: application to the Illgraben debris-flow channel, Earth Surface Process and Landforms, 36, 1847-1859: 2011.

Shan J., Toth K.: Topographic laser ranging and scanning: principles and processing. CRC Press, Taylor & Francis Group, LLC, UK, 2008.

Shepard D.: A two-dimensional interpolation function for irregularly spaced data, New York, USA, 1968.

Shepard D.: A Two-Dimensional Interpolation Function for Irregularly Spaced Data, Proceedings of 23rd ACM National Conference, New York, 1968, 517-523. doi:10.1145/800186.810616, 1968.

Travelletti, J., Sailhac, P., Malet, J.-P., Grandjean, G., Ponton, J. : Hydrological response of weathered clay-shale slopes: water infiltration monitoring with time-lapse electrical resistivity tomography. Hydrological Processes, doi:10.1002/hyp.7983. 2012.

Valentin C., Poesen J., Yong L.: Gully erosion: Impacts, factors and control.Catena 63, (2005) 132-153, 2005.

Yamakoshi T., Mathys N., Klotz S.: Time-lapse video observation of erosion processes on the black marls badlands in the Southern Alps, France. Earth Surface Processes and Landforms 34(2): 314–318, 2009.

Yamakoshi T., Mathys N. and Klotz S.: Visual observation of erosion processes on the Black Marl badlands in the southern Alps, France. In Calcaterra, D. & Parise, M. (eds) Weathering as a Predisposing Factor to Slope Movements. Geological Society, London, Engineering Geology Special Publications, 23, 201–212, 2010.

728

Table 1: Characteristics of the TLS alignment with, for each time period, with the information on the number of scans used to create a scene. The table indicates standard deviation of the point to the surface matched (point to surface ICP), the mean difference between two scans (either used for to align on period or for inter period comparison), the used average point density and the standard deviation of the average mean difference.

	Alignment scans of each period					Inter-period			
Period of time	**Num. scans**	**Std. Dev. Pts.-Surf. [m]**	**Mean diff. align. [m]**	**Pts. Density [pts.cm^{-2}]**	**Std. Dev. Mean diff. [m]**	**Std. Dev. Inter period [m]**	**Mean diff. Inter period [m]**	**Pts. Density [pts.cm^{-2}]**	**Std. Dev. Mean diff. [m]**
May 2007 (O)	3	6.00E-03	1.00E-05	1.26E+00	2.09E-06	1.50E-02	-2.70E-04	7.24E+01	3.40E-05
June 2007 (O)	1	-	-	7.76E-01	-	1.33E-02	-6.00E-05	4.98E+00	1.07E-05
June 2008 (O)	3	7.00E-03	2.00E-05	1.37E+00	2.27E-06	6.94E-03	-1.70E-04	2.62E+00	4.34E-06
April 2009 (O)	6	1.20E-02	3.40E-05	1.49E+00	3.05E-06	5.47E-03	-1.10E-04	-	-
June 2009 (O)	4	4.60E-03	7.00E-05	1.32E+00	1.27E-06	-	-	-	-
Aug. 2009 (O)	7	5.20E-03	8.00E-06	1.59E+00	1.32E-06	5.56E-03	-1.30E-04	-	-
Nov. 2009 (L)	4	4.20E-03	2.00E-05	6.10E-01	1.87E-06	5.20E-03	2.80E-04	-	-
March 2010 (L)	3	3.40E-03	4.30E-05	3.48E-01	2.02E-06	3.85E-03	3.80E-04	-	-
May 2010 (O)	6	4.60E-03	9.00E-06	3.09E+00	7.65E-07	5.17E-03	-8.00E-05	8.69E+00	3.27E-06
June 2010 (O)	6	4.80E-03	7.00E-06	3.26E+00	7.89E-07	5.46E-03	-2.20E-04	9.99E+00	1.52E-06
Sept. 2010 (L)	3	2.60E-03	-2.00E-06	1.79E-01	1.57E-06	5.44E-03	9.29E-03	-	-
Nov. 2010 (L)	3	2.70E-03	3.00E-05	4.09E-01	1.51E-06	4.55E-03	-3.50E-04	-	-

O = LiDAR Optech Ilris 3D L = LiDAR Leica TotalStation II

Table 2: Measured volume of erosion and deposition. In order to perform comparison with table 3, 0.48 m^3 have been added to the first period to the cumulative volume.

Date start	Date end	Density [kg/m3]	Erosion [m3]	Deposit [m3]	Balance [m3]	Vol Cum. [m3]	Vol / year [m3/y]	Erosion rate [mm/y]
14.04.2009	31.05.2009	1500	-0.56	0.27	-0.30	0.78	6.04	4.54
31.05.2009	11.08.2009	2325	-0.38	0.38	-0.01	0.78	0.03	0.02
11.08.2009	03.11.2009	1875	-1.99	1.05	-0.94	1.73	4.09	3.07
03.11.2009	23.03.2010	1875	-4.54	3.34	-1.20	2.92	3.12	2.34
23.03.2010	28.05.2010	1500	-2.74	0.02	-2.72	5.64	15.05	11.32
28.05.2010	23.06.2010	1500	-6.29	0.26	-6.03	11.68	84.71	63.69
23.06.2010	22.09.2010	2325	-0.42	0.05	-0.37	12.04	1.47	1.10
22.09.2010	04.11.2010	1875	-1.78	0.16	-1.62	13.66	13.73	10.33
				Volume added for the 14.4.2009		0.48		

Table 3: Measured volume in the sediment trap.

Date	Measured Volumes [m^3]	Cumulative Volumes [m^3]	Date	Measured Volumes [m^3]	Cumulative Volumes [m^3]
26.01.2009	-	-	13.02.2010	1.42	5.6
09.02.2009	0.48	0.5	05.05.2010	0.01	5.6
17.04.2009	0.67	1.2	07.05.2010	0.01	5.6
05.05.2009	0.02	1.2	11.05.2010	2.87	8.5
02.07.2009	0.20	1.4	17.05.2010	0.01	8.5
10.08.2009	0.09	1.5	16.06.2010	3.31	11.8
20.08.2009	0.02	1.5	24.08.2010	0.49	12.3
27.09.2009	0.03	1.5	13.09.2010	0.08	12.4
28.09.2009	0.24	1.7	22.09.2010	0.02	12.4
22.10.2009	1.72	3.5	27.09.2010	0.32	12.7
04.11.2009	0.61	4.1	05.10.2010	1.74	14.5
06.12.2009	0.12	4.2	25.10.2010	0.01	14.5

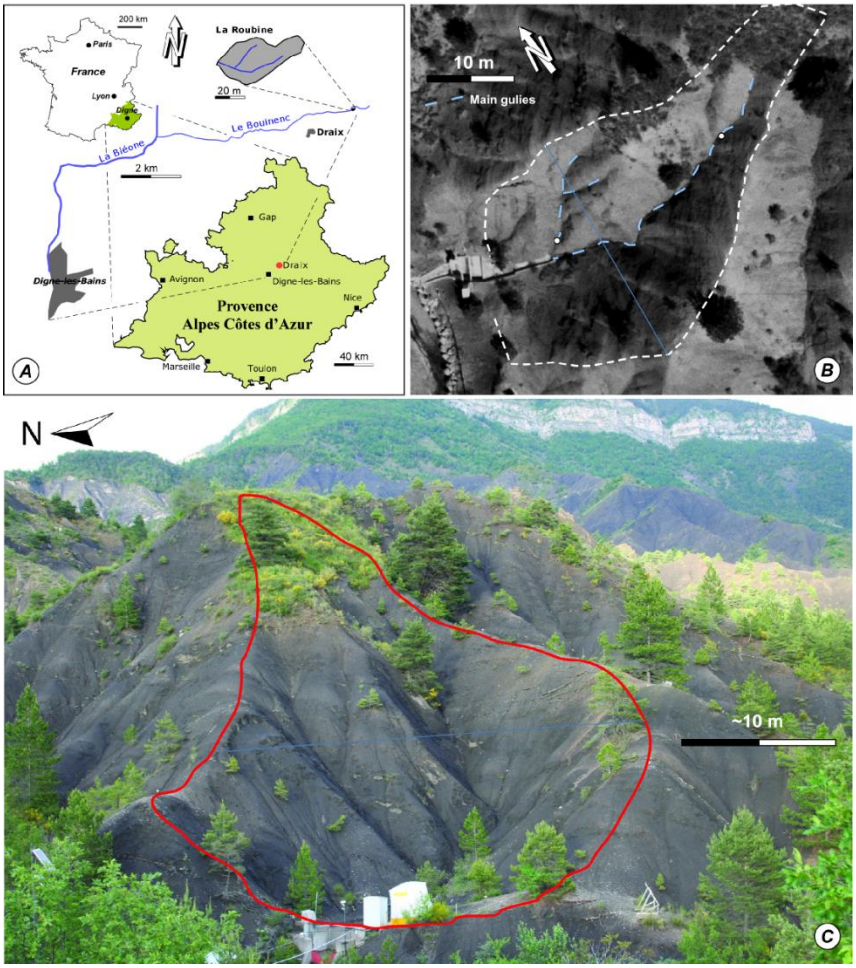

Figure 1: Location and picture of la Roubine. (A) Location of la Roubine catchment (B) Aerial image of La Roubine. (C) Photograph of the Roubine catchment (1/6/2011) with the contours indicated in red line. Foreground: La Roubine catchment characterized by a typical badland morphology, many small scale rills and gullies, steep slopes and scarce vegetation. The catchment outlet is located at the western extremity with the sediment trap and the limnigraph. Background: Surrounding badlands and limestone ridge.

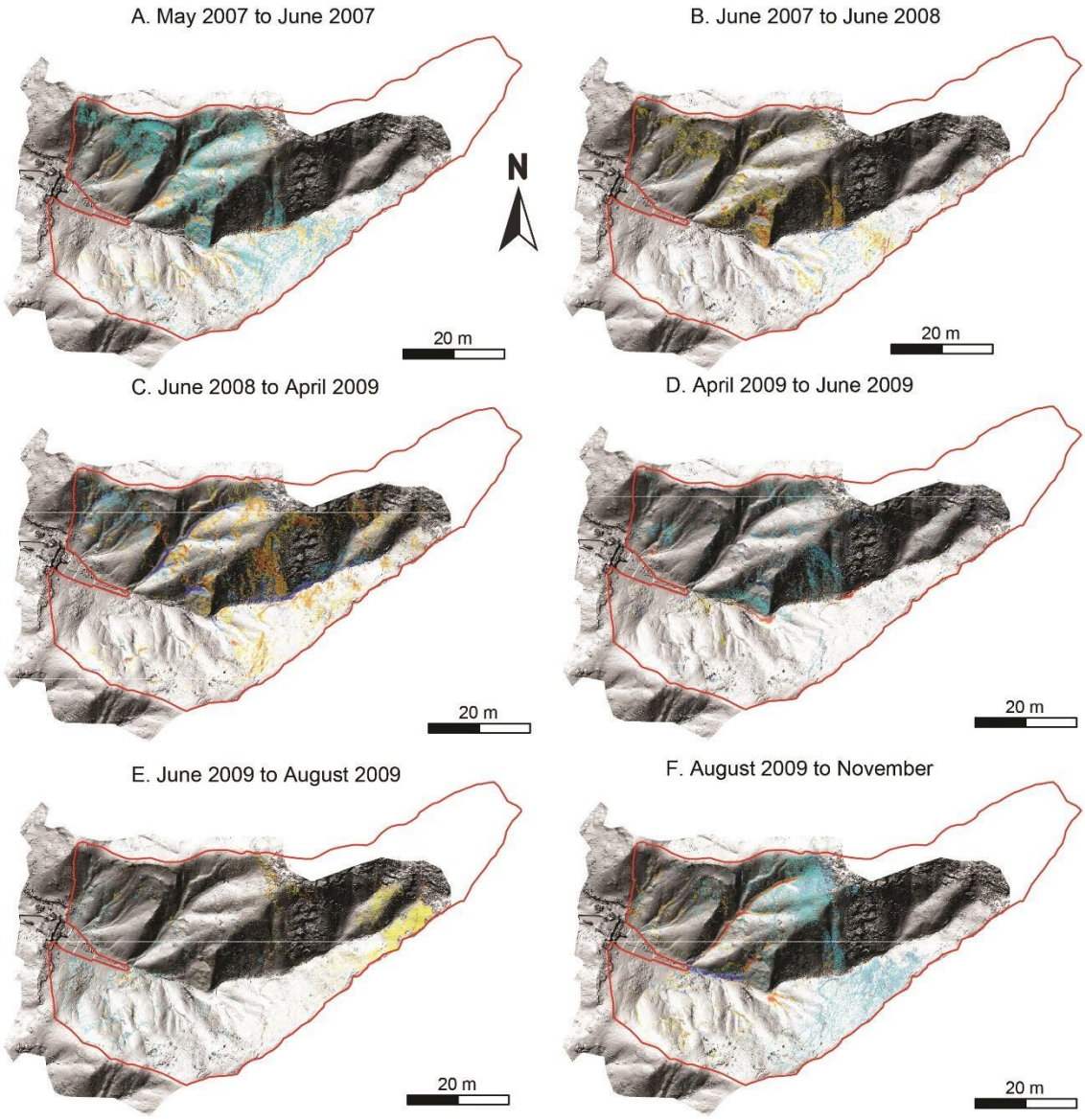

20

21 (cont. next page)

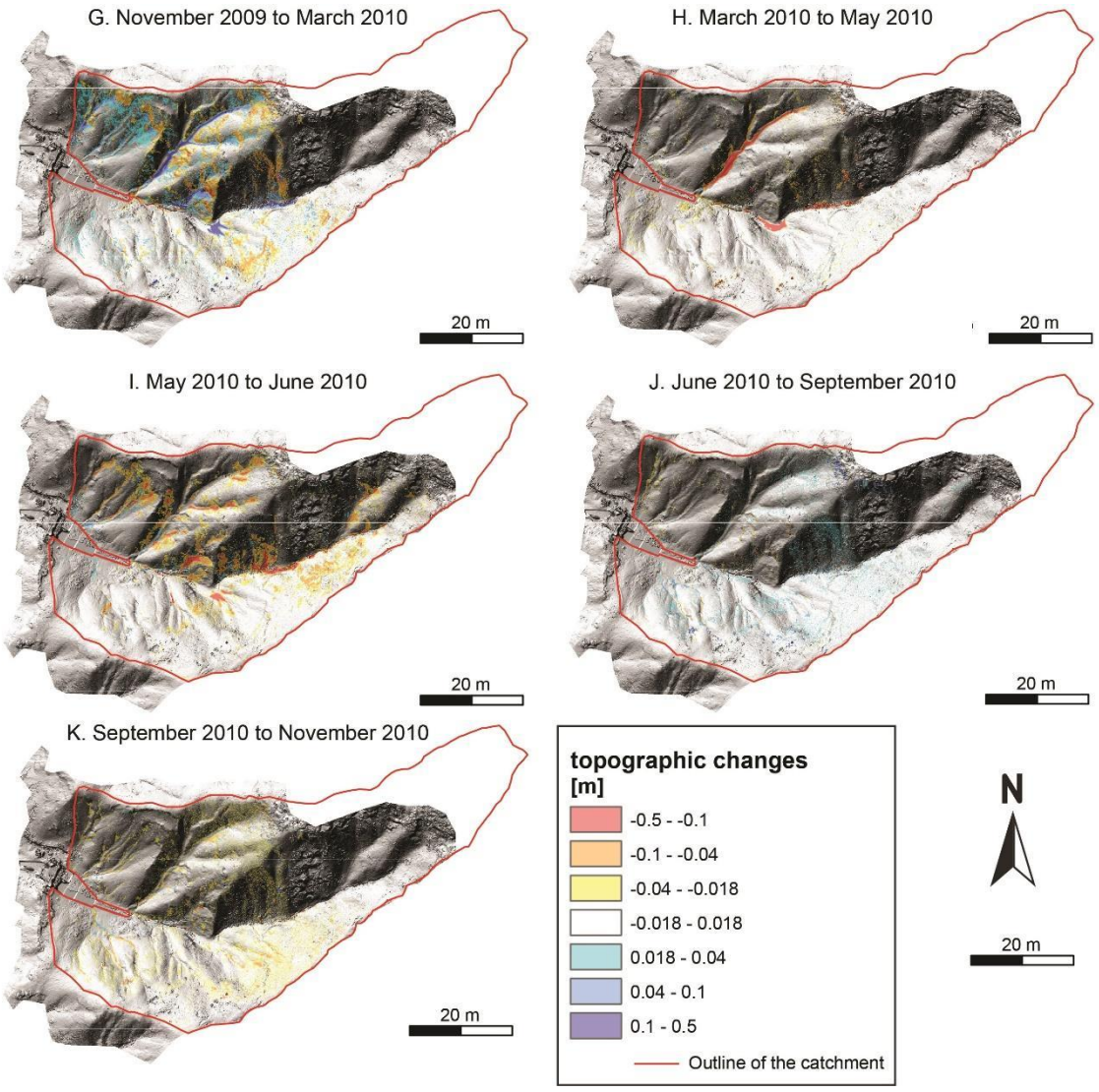

Figure 2: Observed height differences for the period 2007-2010 highlighting the soil surface changes of La Roubine catchment. The red outline indicates the boundary of the catchment (see large version in the supplementary material).

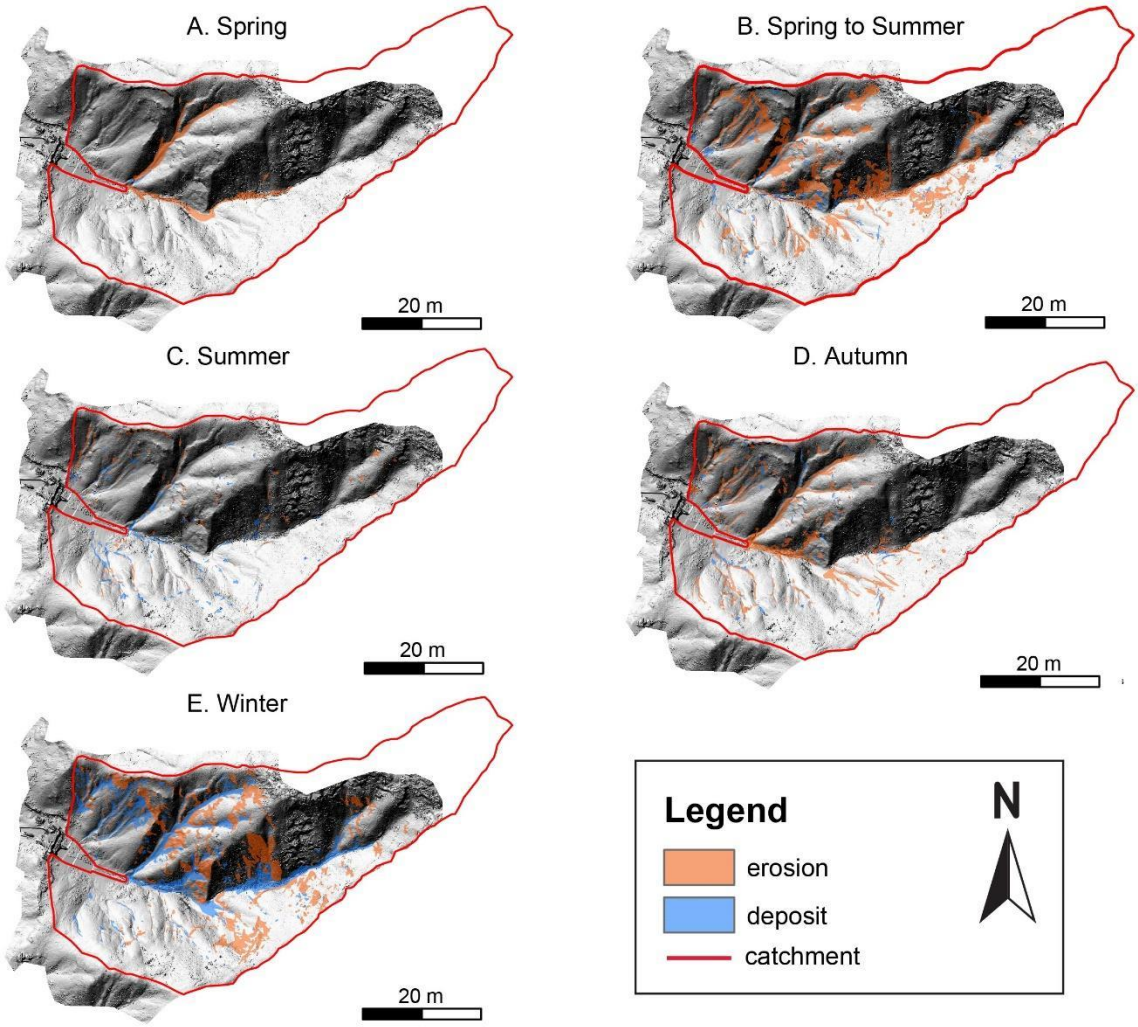

28

29 Figure 3: Typical pattern of slope activity (e.g. erosion in orange, deposition in blue) for
30 each predefined seasons. The red outline indicates the boundary of the catchment (see also
31 the video in the supplementary material).

32

33

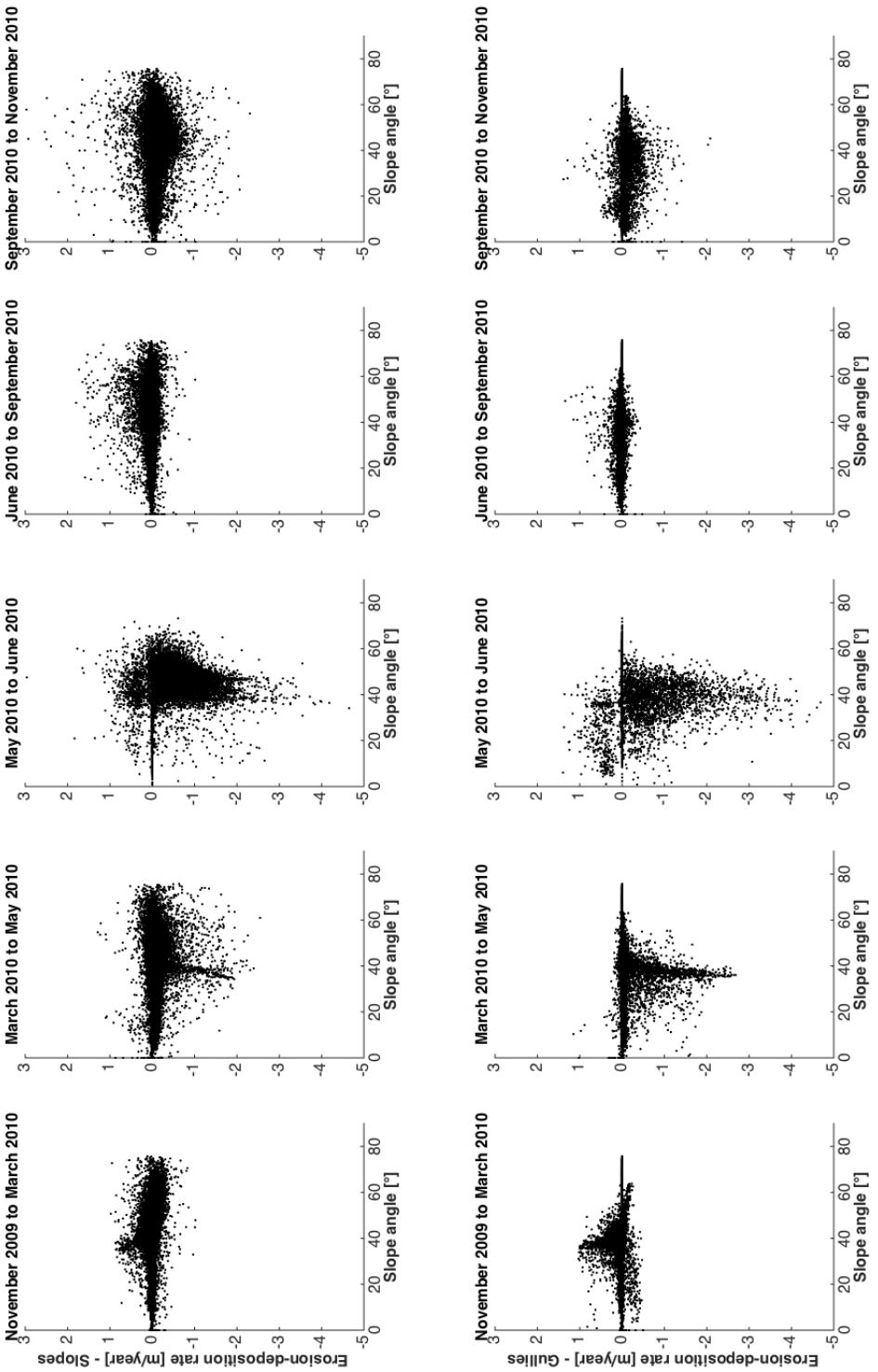

Figure 4: Vertical change over time vs slope angle. Rates are calculated from a 10 cm grid average of original DoDs and divided by the time separating the two LiDAR acquisitions. Slope angle in degrees, calculated in ArcGIS on a 10 cm DEM of June 2010. Top row shows rates for slopes, bottom row for gullies and adjacent (20 cm or closer) pixels (see supplementary material for similar graphs showing vertical change in absolute value vs slope angle).

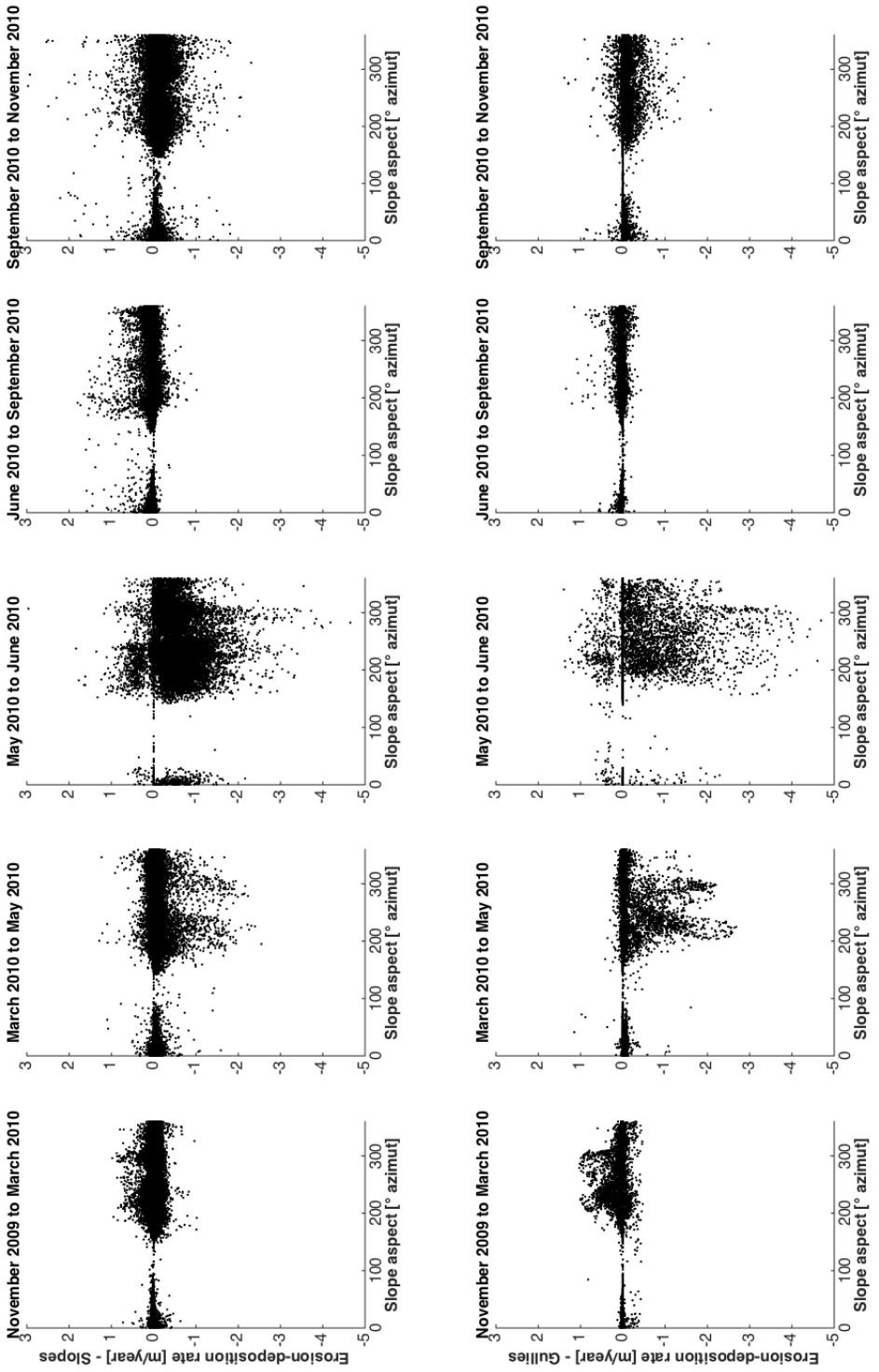

Figure 5: Vertical change over time vs slope aspect. Rates are calculated from a 10cm grid average of original DoDs and divided by the time separating the two LiDAR acquisitions. Slope aspect in degrees, calculated in ArcGIS on a 10 cm DEM of June 2010. Top row shows rates for slopes, bottom row for gullies and adjacent (20cm or closer) pixels (see supplementary material for similar graphs showing vertical change in absolute value vs slope aspect).

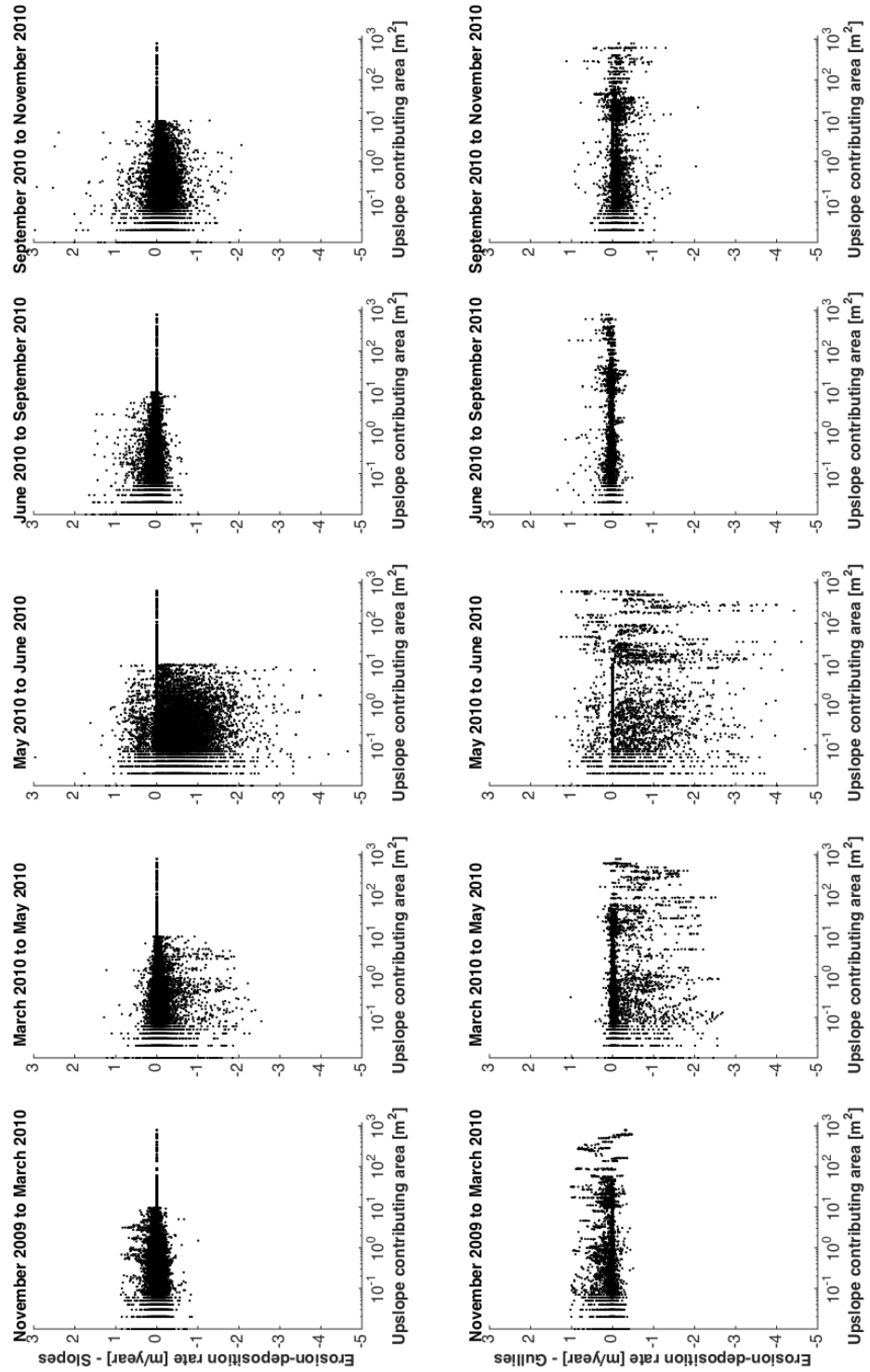

Figure 6: Vertical change over time vs upslope contributing area. Rates are calculated from a 10 cm grid average of original DoDs and divided by the time separating the two LiDAR acquisitions. Upslope contributing area in square meters, calculated in ArcGIS on a 10 cm DEM of June 2010. Top row shows rates for slopes, bottom row for gullies and adjacent (20cm or closer) pixels (see supplementary material for similar graphs showing vertical change in absolute value vs contributing area).

52

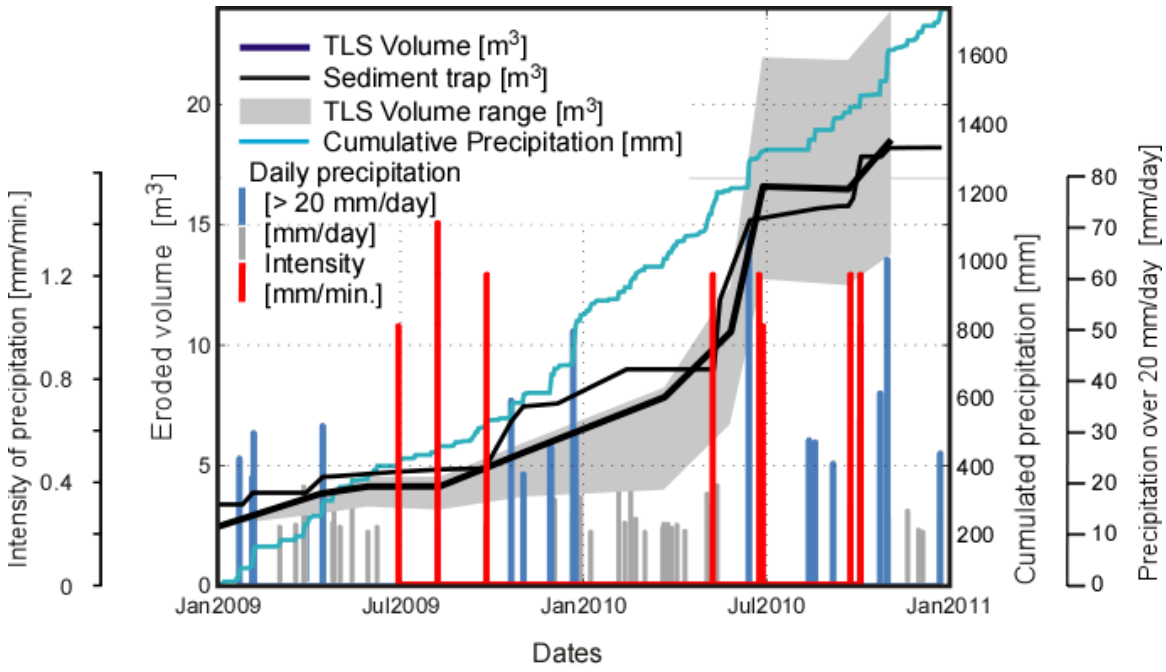

Figure 7: Cumulated TLS measured volumes (in bold black line) against cumulated calibrated on sediment trap measured volumes (thin black line) for the years 2009 and 2010. In addition, the cumulative precipitation are shown as well as the daily precipitations events (in grey) and the main daily precipitation events that are considered as significant in red (>20 mm/day) and the largest intensity event above 10 $mm.min^{-1}$ sampled with a tipping bucket rain gauge. The initial sediment delivery is not zero because we used the storage in the sediment trap of the previous period as initial value.

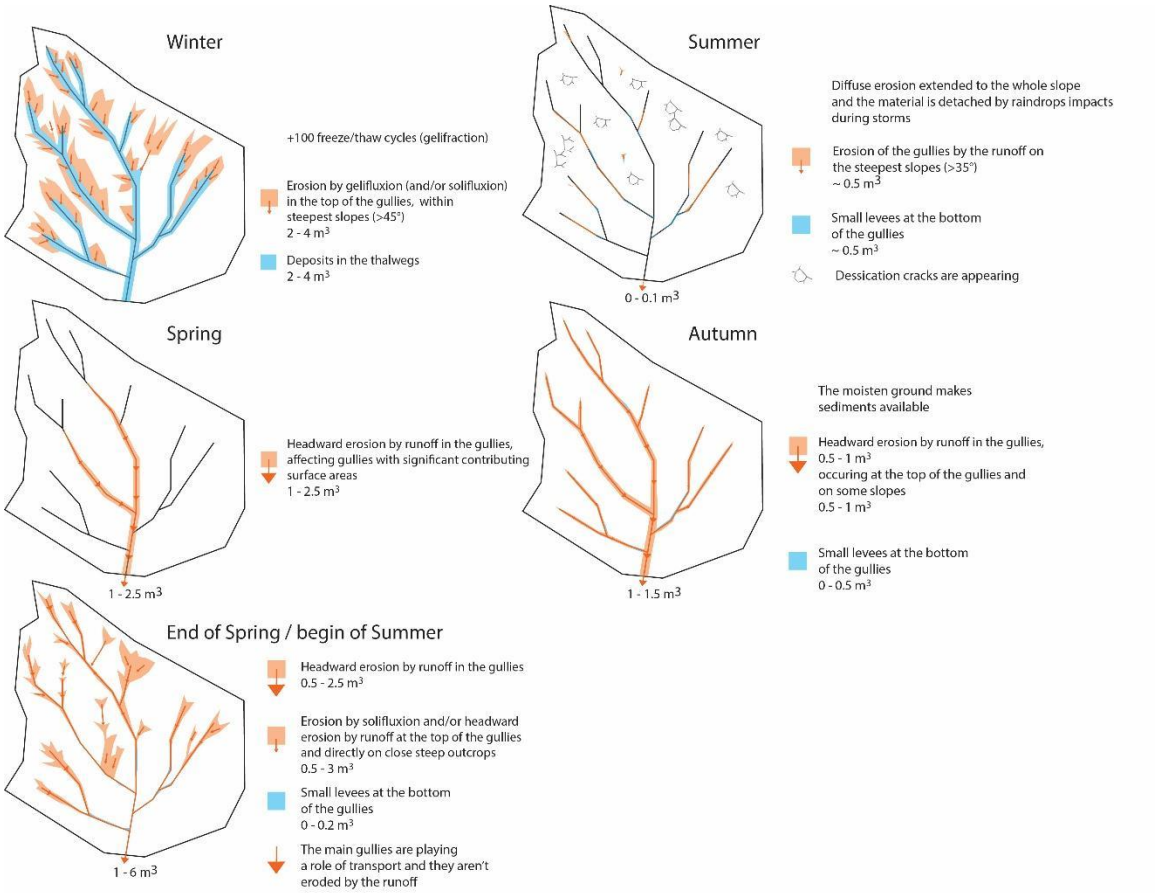

61

62 Figure 8: Conceptual model describing the seasonal pattern of erosion and deposition and
63 quantification of the volumes of sediment transfer at La Roubine catchment.

64